Computational Evaluation of Me2TCCP as Lewis acid

Roeleveld, J.J.; Ehlers, A.W.; Mooibroek, T.J.

DOI
10.1002/cphc.202100426
Publication date
2021
Document Version
Final published version
Published in
ChemPhysChem

Special Collection

Computational Evaluation of Me_2TCCP as Lewis Acid

Julius J. Roeleveld,[a] Andreas Wolfgang Ehlers,[a] and Tiddo Jonathan Mooibroek*[a]

Supramolecular adducts between dimethyl-2,2,3,3-tetracyanocyclopropane (Me_2TCCP) with 21 small (polar) molecules and 10 anions were computed with DFT (B3LYP-D3/def2-TZVP). Their optimized geometries were used to obtain interaction energies, and perform energy decomposition and 'atoms-in-molecules' analyses. A set of 38 other adducts were also evaluated for comparison purposes. Selected examples were further scrutinized by inspection of the molecular electrostatic potential maps, Noncovalent Interaction index plots, the Laplacian, the orbital interactions, and by estimating the Gibbs free energy of complexation in hexane solution. These calculations divulge the thermodynamic feasibility of Me_2TCCP adducts and show that complexation is typically driven by dispersion with less polarized partners, but by orbital interactions when more polarized or anionic guests are deployed. Most Me_2TCCP adducts are more stable than simple hydrogen bonding with water, but less stable than traditional Lewis adducts involving Me_3B, or a strong halogen bond such as with Br_2. Several bonding analyses showed that the locus of interaction is found near the electron poor sp^3-hydridized $(NC)_2C–C(CN)_2$ carbon atoms. An empty hybrid σ^*/π^* orbital on Me_2TCCP was identified that can be held responsible for the stability of the most stable adducts due to donor-acceptor interactions.

Introduction

Fundamental molecular life-processes such as protein folding and molecular recognition are phenomena driven for a large part by non-covalent interactions.[1] Hydrogen bonding (HB)[2] and halogen bonding (HlgB)[1a,3] are among the best known interactions, and both can be seen as a species of the genus 'σ-hole interactions'.[4] The term 'σ-hole' refers to a feature of the electron density around the 'σ-hole donor' atom (D) when bound to another atom (X). This electron density is anisotropic and can have a positive electrostatic potential on the extension (or nearly so) of the X–D bond.[4a,5] The location of this *de facto* Lewis acidic site coincides with the σ* orbital of the X–D bond. The ultimate outcome of a σ-hole interaction can indeed be genuine σ-bond breaking and/or making, such as deprotonations[6] or I^- attack on molecular iodine to form $[I_3]^-$.[6–7]

Following this logic, one can see that in principle any main group element of the periodic table could be rendered a σ-hole donor.[8] For example, σ-hole interactions with elements from the oxygen family have been defined by the IUPAC as Chalcogen bonds in 2019.[9] Experimentally, these chalcogen bonding interactions have been utilized in dithienothiophene derivatives[10] as transmembrane anion transporters,[11] mechanosensitive fluorescent probes,[10,12] and catalysts.[13]

Of all the elements that could function as σ-hole donor, carbon is a most interesting candidate[4b,14] because it is so ubiquitous in synthetic chemistry and of central importance to life itself. The relevance of σ-hole interactions with this member of the tetrel family can be deduced from the canonical S_N2 nucleophilic displacement reaction[4b,15] of Cl^- attacking CH_3I along the vector of the C–I bond; in the course of the reaction there are clear energy minima preceding and following the $[Cl\cdots CH_3\cdots I]^-$ transition state.[15b] Similar interactions involving methyl groups have been noticed to persist in crystal structures[16] and various computational inquiries have affirmed the stabilizing effect of C-centred 'tetrel-bonding' interactions.[16–17] Most of these observations disclose accidental glimpses of the interaction and it remains a challenge to perceive of stable and tenable molecules that can be exploited for their tetrel-bond forming potential.

It has been postulated based on exploratory DFT calculations and an evaluation of crystal structure data that 1,1,2,2-tetracyanocyclopropane (TCCP) rings might be a viable supramolecular synthon for C-centred tetrel-bonding interactions.[18] The electrostatic potential map of dimethyl-TCCP (Me_2TCCP) indeed reveals a clear Lewis acidic site located mainly on the two central C-atoms of the $C_2(CN)_4$ fragment, as is shown in Figure 1a. It has later been demonstrated that TCCP derivatives can direct the positioning of ether fragments by virtue of C···O interactions in the gas phase and in the crystalline state,[19] as exemplified by the crystal structure of [Me_2TCCP···tetrahydrofuran] sown in Figure 1b.[19b] Here, we report on an extensive computational evaluation of Me_2TCCP adducts to gain insight into the stability and preferences of TCCP as Lewis acid towards a variety of anionic and charge neutral Lewis bases.

[a] J. J. Roeleveld, Dr. A. W. Ehlers, Dr. T. J. Mooibroek
van 't Hoff Institute for Molecular Sciences
Universiteit van Amsterdam
Science Park 904, 1098 XH Amsterdam, The Netherlands
E-mail: t.j.mooibroek@uva.nl

Supporting information for this article is available on the WWW under https://doi.org/10.1002/cphc.202100426

An invited contribution to a Special Collection on Molecular Recognition.

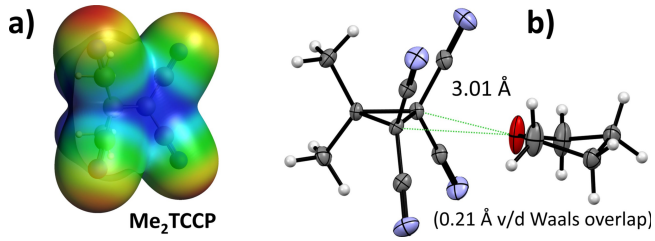

Figure 1. Molecular electrostatic potential map (MEP) of Me_2TCCP (**a**) and illustration of the crystal structure of the [Me_2TCCP···THF] co-crystal (**b**).[19b] The MEP was calculated at the B3LYP-D3/TZ2P level of theory and the colour scale ranges from −31 kcal mol^{-1} (red) to 38 kcal mol^{-1} (blue).

Results and Discussion

As is summarized in Table 1, various Me_2TCCP adducts with polar molecules (entries 1a–k), common solvents (entries 2a–g) and anions (entries 4a–j) were investigated computationally. For comparison purposes, several dimers of linear alkanes were also considered (entries 3a–f). The contribution to ΔE of steric interaction (S), orbital interactions (O) and dispersion (D) was inspected with the energy decomposition analysis implemented in ADF and listed in kcal mol^{-1}. The steric interaction between two fragments is a balance between the Pauli repulsion and electrostatic interactions (i.e., the interaction between the electron density of one fragment and the nuclei of the other and *vice versa*). The orbital interaction is usually dominated by the stabilisation of the high lying occupied orbitals of one fragment by the low lying empty orbitals of the other fragment (donor-acceptor interaction) but also contains the mixing of occupied and empty orbitals at the same fragment (polarisation). Dispersion is the interaction from induced dipoles resulting in a temporarily attractive force. Energy decomposition analyses of small molecular adducts[20] have proven to be useful to probe the physical origins of hydrogen[16b,21] and halogen[22] bonding. An atoms-in-molecules (AIM) analysis was also conducted and Table 1 lists the densest bond critical points obtained for each adduct (ρ in 10^2 a.u.), with a specification of the atoms involved. Graphical representations of the adducts and the AIM analyses of all adducts listed in Table 1 are shown in Figure S1.

The interaction energy of the Me_2TCCP dimer is already fairly favourable by ΔE = −7.9 kcal mol^{-1} (entry 1a) and held together by several polar interactions involving the nitrile groups (see Figure S1). Dispersion is the main driving force (−7.8 kcal mol^{-1}), followed by orbital interactions (−2.8 kcal mol^{-1}), which is balanced with steric repulsion. The interaction energies of Me_2TCCP with small molecules of single bonded O, S, N or P bearing a lone-pair (entries 1b–e) are more favourable than the dimer (between −8.9 and −9.7 kcal mol^{-1}) and dispersion typically is again the main driving force. However, orbital interactions can be more substantial than in the dimer (up to −4.1 kcal mol^{-1} for Me_3N, entry 1d-1). In all cases, the lone-pair bearing atom is pointing towards the Lewis acidic site of Me_2TCCP, as is exemplified for [Me_2TCCP···OMe_2] and [Me_2TCCP···NMe_3] in Figure 2a and 2b respectively.

Of these adducts (entries 1b–e) [Me_2TCCP···NMe_3] is the most stable one at −10.4 kcal mol^{-1} (entry 1d-1) and the N-atom is pointing towards the Lewis acidic site in Me_2TCCP.

Table 1. Numerical overview of geometry optimized adducts, their interaction energy (ΔE, kcal mol^{-1}, from energies of geometries within the adduct),[a] an energy decomposition analysis (into sterics (Pauli repulsion + electrostatic interaction), orbital interactions and dispersion) and an 'atoms-in-molecules' analysis (AIM). See Figure S1 for geometries and AIM analyses.

Entry	partner	ΔE[a]	S/O/D [b]	AIM[c]	Entry	partner	ΔE[a]	S/O/D [b]	AIM[c]
1a	Me_2TCCP	−7.9	2.7/−2.8/−7.8	0.6 (N···C)	**2g**	*n*-C_5H_{12} (*n*-Pen)	−5.1	4.1/−1.8/−7.4	0.4 (6× H···CN)
1b	OMe_2	−9.7	0.0/−3.1/−6.6	1.0 (O···C)	**2h**	*n*-C_4H_{10} (*n*-But)	−4.9	3.7/−1.6/−6.9	0.4 (6× H···CN)
1c	SMe_2	−9.3	1.2/−3.3/−7.2	0.7 (S···C)	**3a**	$(C_6H_{14})_2$	−5.8	3.9/−1.8/−7.9	0.5 (12× H···H)
1d-1	NMe_3 [d]	−10.4	1.8/−4.1/−8.5	0.8 (N···C)	**3b**	$(C_5H_{12})_2$	−3.7	3.1/−1.2/−5.6	0.5 (9× H···H)
1d-2	NMe_3 [d]	−3.9	3.4/−1.7/−5.5	0.8 (N···C)	**3c**	$(C_4H_{10})_2$	−2.0	2.7/−1.2/−3.5	0.5 (7× H···H)
1e	PMe_3	−8.9	1.2/−3.6/−6.5	0.8 (P···C)	**3d**	$(C_3H_8)_2$	−1.4	1.9/−0.8/−2.5	0.5 (6× H···H)
1f	O=NMe_3	−16.7	−1.0/−8.5/−7.1	1.5 (O···C)	**3e**	$(C_2H_6)_2$	−1.6	1.3/−0.5/−2.4	0.4 (4× H···H)
1g	S=NMe_3	−12.4	0.3/−5.3/−7.4	0.8 (S···C)	**3f**	$(CH_4)_2$	−0.6	0.4/−0.2/−0.8	–
1h	Se=NMe_3	−12.4	1.8/−6.0/−8.2	0.8 (Se···C)	**4a**	Cl^-	−24.1	−1.5/−18.5/−4.1	1.5 (Cl···C)
1i	O=PMe_3	−15.3	−1.7/−6.0/−7.6	1.3 (O···C)	**4b**	Br^-	−20.8	−0.1/−15.9/−4.8	1.2 (Br···C)
1j	S=PMe_3	−11.3	1.7/−4.8/−8.2	0.8 (S···C)	**4c**	I^-	−16.3	2.0/−13.0/−5.3	1.0 (I···C)
1k	Se=PMe_3	−11.8	2.3/−5.3/−8.8	0.8 (Se···C)	**4d**	$N{\equiv}C^-$	−22.5	−3.5/−16.0/−3.0	1.3 (C···C)
2a	O=SMe_2 (DMSO)	−13.3	−0.6/−5.3/−7.4	1.2 (O···C)	**4e**	N_3^-	−22.7	−1.3/−17.8/−3.6	1.7 (N···C)
2b	OC_4H_8 (THF)	−11.2	0.0/−4.4/−7.2	1.2 (O···C)	**4f**	NO_3^-	−21.4	−0.1/−16.1/−5.2	1.4 (3× O···CN)
2c	O=CMe_2 (Acetone)	−10.0	−0.3/−3.6/−6.1	1.1 (O···C)	**4g**	$MeCO_2^-$	−29.0	−0.1/−22.7/−5.8	1.7 (4× O···CN)
2d	PhMe (Tol)	−8.6	3.4/−2.6/−9.4	0.6 (4× C···CN)	**4h**	ClO_4^-	−16.2	1.3/−11.0/−6.5	1.2 (3× O···CN)
2e	CH_2Cl_2 (DCM)	−5.8	2.7/−2.1/−6.4	0.6 (Cl···C)	**4i**	BF_4^-	−16.2	−0.5/−10.8/−4.9	1.2 (4× F···CN)
2f	*n*-C_6H_{14} (*n*-Hex)	−5.6	4.2/−2.0/−7.9	0.4 (6× H···CN)	**4j**	PF_6^-	−12.8	1.4/−8.1/−6.0	1.1 (4× F···CN)

[a] The reported gas-phase interaction energies (ΔE) were computed by ADF at the B3LYP-D3/TZ2P level of theory by subtracting the energies of the individual components from the energy of the adduct. The adduct was geometry optimized in Spartan at the B3LYP-D3/def2-TZVP level of theory. The reported energies and the energy calculated with Spartan by subtracting the energies of geometry optimized components form that of the adduct correlate very well (r^2 = 0.98) as shown in Figure S2, which means that the deformation energy is typical very small. [b] The energy decomposition and atoms-in-molecules analyses were done on these geometries with ADF at the B3LYP-D3/TZ2P level of theory and split up into sterics (S), which is the sum of the electrostatic interaction and Pauli repulsion, orbital interactions (O) and dispersion (D).). [c] The density (ρ in a.u. × 10^2) of the densest bond-critical point(s) are listed. These densities have a reasonable correlation (R^2 = 0.86) with ΔE, as can be seen in Figure S3. Indicated in brackets are the atom of the 'guest' and the sp^3-C or C≡N of Me_2TCCP involved in the b.c.p. (in the linear alkanes all b.c.p.'s are between two H-atoms). [d] In one geometry (entry 1d-1) the N-atoms it facing towards the Lewis acidic site of Me_2TCCP, while in the other (entry 1d-2) the N-atom is facing the opposite way.

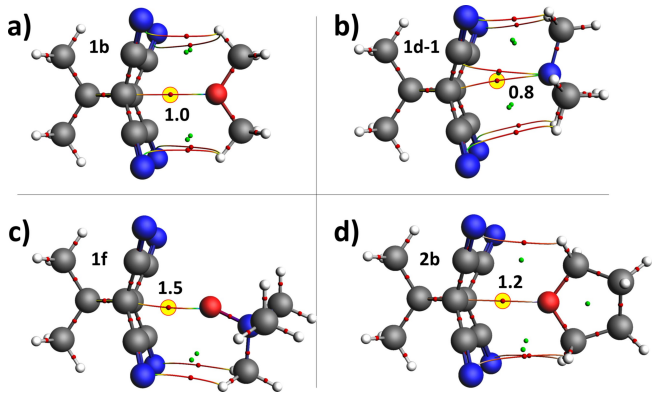

Figure 2. Ball and sticks representations of several charge neutral Me_2TCCP adducts that were geometry optimized with DFT at the B3LYP-D3/def2-TZVP level of theory. The thin red lines and small spheres respectively represent the bond paths and bond critical points (b.c.p.) of an 'atoms-in-molecules' analysis. The b.c.p.'s with an sp^3-C of Me_2TCCP are highlighted in yellow and the density of this point is indicated (ρ in a.u. $\times 10^2$).

Rotating the trimethylamine so that the N-atom is pointing away from Me_2TCCP (entry 1d-2) results in a very weak adduct ($\Delta E = -3.9$ kcal mol^{-1}) held together by various weak CH···CN interactions, which are mostly dispersive in nature.

Adducts of chalcogenated trimethylamine (entries 1f–h) and trimethylphosphane (entries 1i–k) (double bonded O, S, Se) are even more stable (between -11.3 and -16.7 kcal mol^{-1}). The orbital contribution is even larger with these more polar molecules (between -4.8 and -8.5 kcal mol^{-1}) and becomes actually the main driving force in the $Me_3N{=}O$ adduct (entry 1f). The geometries of these adducts are essentially isostructural (Figure S1), with the chalcogen atom pointing towards the Lewis acid site of Me_2TCCP. This is exemplified for the [$Me_2TCCP{\cdots}ONMe_3$] adduct shown in Figure 2c. The interaction energies are largest for the oxygenated species (entries 1f and 1i) while the sulphur and selenium compounds have about the same ΔE. This is likely due to the larger electronegativity of O (3.44) *versus* S (2.58) and Se (2.55).[23]

The interaction energies with several common solvents (entries 2a–g) are also negative and the energetic details are very similar to those described above for other small polar (chalogenated) molecules. As an example, Figure 2d shows the [$Me_2TCCP{\cdots}THF$] adduct, which has also been observed experimentally using rotational spectroscopy.[19b] The adducts with linear alkanes (entries 2f–h) are reasonably stable at about -5 kcal mol^{-1}, which is mainly due to dispersion and actually sterically unfavourable by about $+4$ kcal mol^{-1}. The relatively large interaction energies between Me_2TCCP and linear alkanes is likely due to the large contact surface, which is about the same in all three adducts with linear alkanes (see also Figure S1).

For comparison purposes, dimers of several linear alkanes were evaluated, as listed in entries 3a–f. The interaction energy of the *n*-hexane dimer (entry 3a) is similar to its adduct with Me_2TCCP (entry 2f-1) and both are less stabilised than the Me_2TCCP dimer. As can be expected,[24] ΔE of the alkane dimers becomes less favourable as the alkanes become shorter and all adducts are dominated by dispersion and sterically disfavoured. ΔE is less effected by shortening the alkyl chain in the Me_2TCCP adduct (entries 2f–h). This is likely because the effective contact surface between Me_2TCCP and hexane, pentane or butane hardly changes (see Figure S1).

The interaction energies of adducts with various anions (entries 4a–j) are much more favourable than those with neural molecules and range from -12.8 kcal mol^{-1} with PF_6^- to -28.5 kcal mol^{-1} with $MeCO_2^-$. In the optimized geometries (Figure S1), all anions are located near the Lewis acidic site with one or two electron rich atoms pointing towards the central sp^3-C atoms. This is exemplified for the adducts with a Cl^-, CN^-, AcO^-, and BF_4^- anion in Figure 3a–d respectively. Interestingly, the magnitude of the steric interaction (about ± 2 kcal mol^{-1}) and the dispersion (about -5 kcal mol^{-1}) is similar as was observed in the charge-neutral adducts. In sharp contrast, the contribution from orbital interactions is much larger (up to -23 kcal mol^{-1} for $MeCO_2^-$, entry 4g) being the leading contribution in all anionic adducts. Moreover, the orbital interactions are lowest for the relatively non-coordinating or 'soft' anions I^-, ClO_4^-, BF_4^- and PF_6^- (below about -16 kcal mol^{-1}).

As listed in Table 2, two series of calculations were performed (entries 1 and 3) for comparison to adducts with Me_2TCCP (entry 2). The first series concerns OMe_2, SMe_2, NMe_3 or PMe_3 as the electron rich partner for several electron deficient molecules (entries 1-1 to 1-7 and Me_2TCCP in entry 2). These calculations were conducted to contextualize the Me_2TCCP adducts with well-known types of interactions. For example, water was used to model hydrogen bonding (entry 1-2), trimethylborane was used as a classical Lewis acid (empty p-orbital, entry 1-2), and molecular bromine was used as a typical halogen bond donor (entry 1-3). Methyliodide and methylbromide were also considered, both as halogen bond donor (entries 1-4 and 1-5) and a tetrel-bond donor (entries 1-6 and 1-

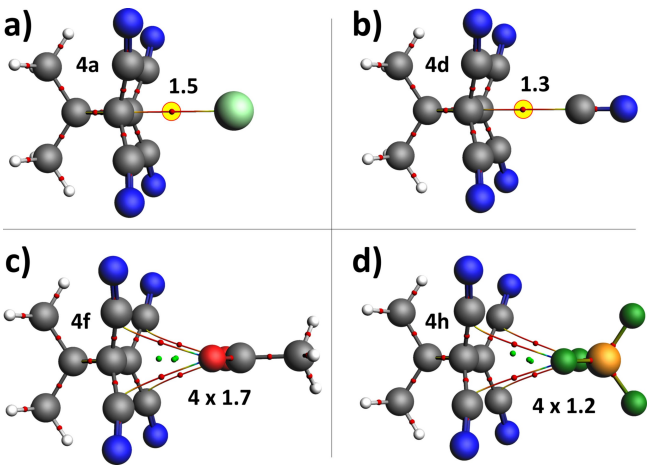

Figure 3. Ball and sticks representations of several anionic Me_2TCCP adducts that were geometry optimized with DFT at the B3LYP-D3/def2-TZVP level of theory. The thin red lines and small spheres respectively represent the bond paths and bond critical points (b.c.p.) of an 'atoms-in-molecules' analysis. The b.c.p.'s with an sp^3-C of Me_2TCCP are highlighted in yellow and the density of b.c.p.'s are indicated (ρ in a.u. $\times 10^2$).

Table 2. Overview of adducts between electron rich 'donor' molecules and several 'acceptor' molecules. See Figure S5 for geometries and AIM analyses.

entry	Donor → Acceptor ↓	OMe_2 [ΔE ; AIM] S/O/D[a]	SMe_2	NMe_3	PMe_3	Cl^-
1-1	HO–H	−6.7 (3.1) −0.4/−4.7/−1.6	−5.9 (2.0) 0.5/−4.4/−2	−9.0 (3.8) 0.8/−7.6/−2.2	−5.4 (2.0) 0.1/−4.4/−1.0	
1-2	Me_3B[b]	−7.5 (2.0) 5.5/−7.2/−5.9	−16.0 (6.0) 31.9/−41.9/−6.8	−35.5 (8.6) 33.3/−61.0/−7.8	−37.2 (11) 61.1/−91.1/−7.2	
1-3	Br–Br[c]	−7.6 (2.8) 3.8/−8.8/−2.5	−14.4 (4.2) 15.1/−26.9/−2.6	−18.6 (8.5) 12.0/−26.7/−3.9	−38.9 (9.2) 65.5/−101.2/−3.2	
1-4	CH_3–I	−1.7 (2.7) 6.9/−5.8/−2.8	−3.9 (1.1) 1.8/−2.9/−2.8	−4.1 (3.3) 10.2/−10.3/−4.0	−4	
1-5	CH_3–Br	−2.5 (1.0) 1.1/−1.3/−2.3	−2.9 (0.7) 1.4/−1.6/−2.7	−3.7 (1.5) 2.3/−3.2/−2.9	−2.0 (0.8) 1.3/−1.7/−1.6	
1-6	I–CH_3	−2.2 (0.7) 1.0/−0.9/−2.3	−2.1 (0.6) 0.8/−0.9/−2.1	−2.7 (0.9) 1.3/−1.4/−2.6	−2.0 (0.6) 0.6/−1.1/−1.4	
1-7	Br–CH_3	−2.6 (0.9) 0.9/−1.1/−2.4	−2.4 (0.6) 1.3/−1.2/−2.5	−3.0 (0.8) 1.0/−1.4/−2.5	−2.2 (0.6) 0.4/−1.2/−1.4	
2-1	Me_2TCCP	−9.7 (1.0) 0.0/−3.1/−6.6	−9.3 (0.7) 1.2/−3.3/−7.2	−10.4 (0.8) 1.8/−3.7/−8.5	−8.9 (0.8) 1.2/−3.6/−6.5	−24.1 (1.5) −1.5/−18.5/−4.1
2-2	Me_2TCCP[d]	−5.6 (1.5) 0.45/−2.2/−3.8				
2-3	Me_aTCCP[e]	−4.1 (0.7) -0.1/−1.1/−2.9				
3-1	Me_2TFCP	−3.8 (1.0) 1.1/−1.1/−3.3				−3.5 (0.8) 5.5/−6.1/−1.9
3-2	Me_2CP	−3.5 (0.8)[f] 1.3/−1.3/−3.3				−3.8 (0.5) 3.6/−4.6/−1.3

[a] see notes [a]–[c] of Table 1; [b] The C_3^{plane} to B distances are respectively: 0.144; 0.337; 0.464; 0.453, with the difference between donors PMe_3 and OMe_2 = 0.453−0.144 = 0.309 Å; [c] The Br–Br bond distance are respectively: 2.347; 2.432; 2.422; 2.658, with the difference between donors PMe_3 and OMe_2 = 2.658−2.347 = 0.311 Å; [d] Starting from a geometry with C–CH_3···O angle of 180° have this geometry which is hydrogen bonded to one CH_3 hydrogen; [e] Geometry with O bifurcated between the two methyl carbon atoms; [f] geometry converged to a hydrogen bonding geometry where O is pointing away from the C_2H_4 centre.

7). An overview of the optimized geometries together with an AIM analysis is given in Figure S5.

With dimethyl ether as electron donor (column 'OMe_2'), Me_2TCCP gave the most stable adduct compared to the other acceptor molecules in the series listed in Table 1. With the other three donors considered, the most stable adducts are obtained with BMe_3 (entry 1-2) and Br_2 (entry 1-3) and follow the order $OMe_2 < SMe_2 < NMe_3 < PMe_3$. This same order is observed for the density of the bond critical point between B/Br and O/S/N/P, which are as large as about 10 (ρ in a.u. $\times 10^2$). Moreover, the C_3^{plane}–B and the Br–Br distances of the OMe_2 adducts are elongated by about 0.3 Å in the PMe_3 adducts (see footnotes b and c of Table 2). Such large structure perturbations of the individual molecules in the adducts, as well as the large bond critical point densities were only observed for BMe_3 and Br_2. These observations are in line with the very large orbital interactions of up to −101 kcal mol^{-1} in [Br_2···PMe_3], and together imply a significant amount donor-acceptor interaction with the empty p-orbital on B and the empty σ* orbital on Br.

Besides the Me_3B and Br_2, the most stable adduct was always observed with Me_2TCCP, even when compared to hydrogen bonding with water (entry 1-1). This can in part be rationalized by the relatively large amount of surface contact, thus always adding a significant amount of stabilization energy due to dispersion.

Interestingly, with nearly all adducts in entries 1-4 to 1-7, the orbital interactions are approximately counteracted by steric repulsion. With OMe_2 as partner to Me_2TCCP (entry 2-1) and with water (entry 1-1) on the other hand, the orbital interactions are at least about 2 kcal mol^{-1} more stabilizing than the sterics are repulsive. This hints at a significant contribution of donor-acceptor interactions, which are smaller than was observed with Me_3B and Br_2. When starting from a [Me_2TCCP·OMe_2] geometry with a C–CH_3···O angle of 180° (entry 2-2), a geometry was obtained where the O is hydrogen bonded by a methyl C–H instead of a tetrel bonding geometry. For a geometry with a bifurcated $(H_3C)_2$···O geometry (entry 2-3), a tetrel bonding geometry was obtained that was about 5.6 kcal mol^{-1} less stable than the $((CN)_2C)_2$···O geometry (entry 2-1). The data with OMe_2 in entry 2 thus implies that the methyl groups on Me_2TCCP are poor electron poor partners.

Another series of adducts was considered between OMe_2 or Cl^- and adapted versions of Me_2TCCP. In dimethyl-1,1,2,2-tetrafluorocyclopronane (Me_2TFCP, entry 3-1), the electron withdrawing cyano substituents on the C3 ring were substituted by fluorines. In dimethylcylclopropane (Me_2CP, entry 3-2), these cyano groups have been replaced by hydrogen atoms. In both cases, the resulting OMe_2/Cl^- adducts are rather weak at less than −4 kcal mol^{-1}. The small interaction energies with Me_2TFCP are consistent with the much smaller electropositive potential (MEP) on the cyclopropane C–F_2 centres of +14 versus +44 kcal mol^{-1} for Me_2TCCP (see Figure S4 for MEP maps). Interestingly, the orbital interactions of the adducts with Me_2TFCP are nearly fully compensated by steric repulsion. The MEP map of Me_2CP actually reveals a small negative potential on the cyclopropane H_2C–CH_2 group fragment (−17 kcal mol^{-1},

see Figure S4). The [$Me_2CP\cdots OMe_2$] adduct converged to a hydrogen bonded geometry, where O is not at all near the H_2C–CH_2 carbon nuclei (see Figure S1). Surprisingly, the [$Me_2CP\cdots Cl^-$] adduct converged at a structure where the Cl^- anion is in close contact with both of the H_2C–CH_2 carbon atoms. Orbital interactions are the major component in all three Cl^- adducts. The calculations with this second series indicate that the cyano groups are important to obtain very stable adducts and that orbital interactions are an important factor. To further unravel the nature of binding with these cyclopropane derivatives, we conducted various bonding analyses.

One of the earlier described bonding analyses are the atoms-in-molecules analyses of the Me_2TCCP adducts. These typically reveal a clear bond critical point (b.c.p.) between an electron rich atom and the cyano C, or the central sp^3-C atom(s) of Me_2TCCP. Actually, the bond paths with sp^3-C atoms are typically directed towards the C–C midpoint and bend toward the C-atoms only very close to the atom (a common artefact when symmetry is not imposed). The density of these b.c.p.'s correlates reasonably well with the stability of the adduct ($R^2 = 0.86$, see also Figure S3). This is in line with earlier reports that the density of a b.c.p. is indicative of the strength of a bonding interaction.[19,25] For larger interacting partners, various weaker hydrogen bonding-like interactions are typically present with b.c.p. densities around 0.4–0.6 (see e.g. the chalcogenated compounds, 1f–k in Figure S1). Interestingly, the AIM analyses with molecular non-linear anions (NO_3^-, AcO^-, ClO_4^-, BF_4^-, PF_6^-) reveal b.c.p.'s with the four cyano C's (see e.g. Figure 3). This raises the question what exactly the bonding mechanism is in anionic Me_2TCCP adducts, for example whether Me_2TCCP adducts are held together by interactions with the sp^3-C atoms of the cyclopropane ring, the sp-C atoms of the cyano groups, or some combination of both. To this end, the Me_2TCCP adducts with AcO^- and Cl^- (entries 4a and 4g in Table 1), as well as the Cl^- adducts with Me_2TFCP (entry 3-1 in Table 2) and Me_2CP (entry 3-2 in Table 2) were scrutinized further (while imposing appropriate symmetry to easy the analysis). Non-covalent interaction (NCI) plots were rendered, cut-planes of the Laplacians were projected on the cyclopropane ring-planes, and the orbital interactions were inspected in detail. The NCI plots shown in the top of Figure 4 clearly show that in all cases the locus of interaction is between the anion and two carbon atoms of the cyclopropane ring.

This is also in the case with the acetate anion, contrary to what the AIM analyses suggest. The deep blue region observed for both Me_2TCCP adducts signifies that the interaction is strongly attractive. This interaction is much weaker in [$Me_2TFCP\cdots Cl^-$] with some dispersive or repulsive interaction regions between Cl^- and the four F-atoms (orange/red).

The NCI-plot for [$Me_2CP\cdots Cl^-$] suggests mostly dispersive or repulsive interaction (orange/red). Shown in the middle of Figure 4 are projections of the Laplacian featuring the typical T-shaped bond path in the case of halides.[26] NCI plots and projections of the Laplacians for other anionic as well as several neutral adducts are shown in Figure S7 and reveal similar trends as with the adducts shown in Figure 4.

Shown in the bottom of Figure 4 are the orbitals resulting from a lone pair of electrons (n) donating into an empty orbital of the cyclopropane rings. The contribution of these interactions decrease in the order: [$Me_2TCCP\cdots AcO^-$]

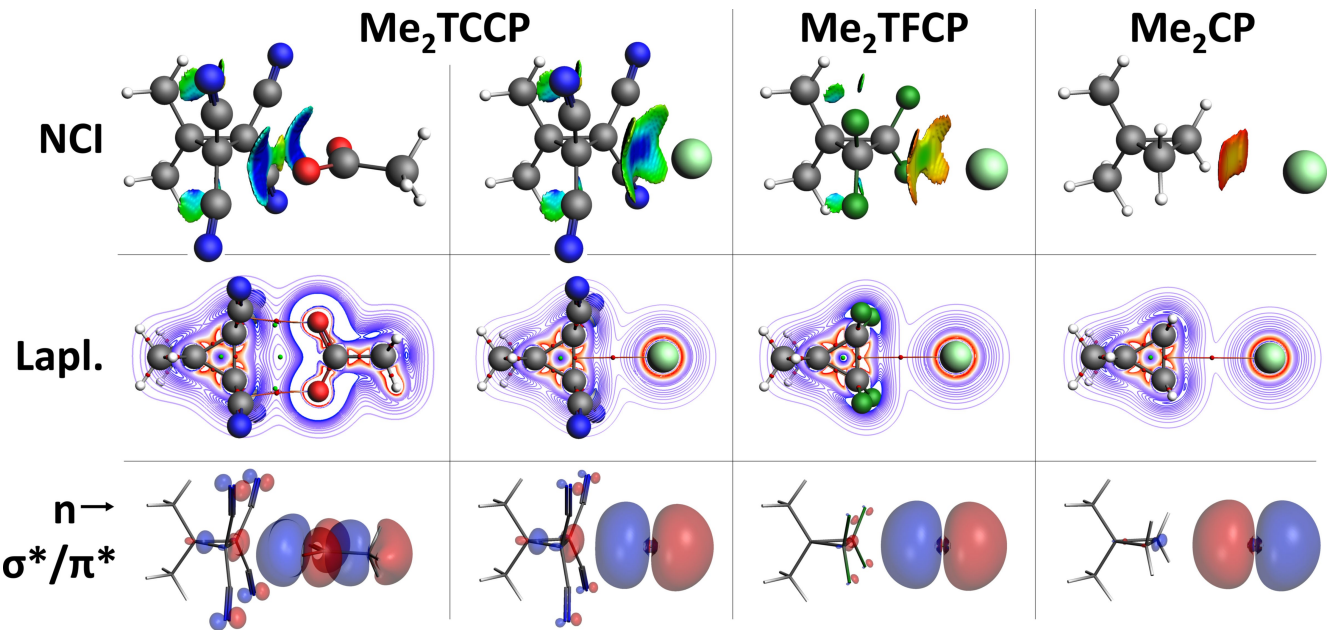

Figure 4. Analyses of the bonding between $CH_3CO_2^-$ or Cl^- and cyclopropane derivatives. Top: noncovalent interaction (NCI) plots, colour coded from 0.003 (red) to 0.015 (blue) a.u. where larger values indicate stronger attraction. Middle: Projection of the Laplacian on the C_2Cl plane colour coded from −0.05 (red) to 0.02 (blue) a.u. in 50 increments. This scaling was chosen based on the [$Me_2TCCP\cdots$*n*-hexane] adduct, which has no overlapping lines on this scale (see Figure S7). The AIM analysis is also shown in this figure (see also Figure S1). Bottom: the bonding orbital of the adduct arising from electron donation of a p-orbital of Cl^- (n) into an antibonding (σ*/π*) orbital of the cyclopropane derivative.

(-22.1 kcal mol^{-1}) > [Me_2TCCP···Cl^-] (-18.0 kcal mol^{-1}) > Me_2TFCP (-6.1 kcal mol^{-1}) > of Me_2CP (-4.6 kcal mol^{-1}). This is in line with an earlier report on the detrimental effect of –C≡N to –F mutation, despite a similar electron withdrawing effect of both –C≡N and –F.[18,27] Most informative is the analysis of the C_2v symmetric [Me_2TCCP···Cl^-] adduct which allows to distinguish the orbital interaction within the irreducible representations. The main contribution of -7.4 kcal mol^{-1} originates from the sigma donation (0.08 e$^-$) of the Cl^- sp-hybrid orbital into the accepting orbital of Me_2TCCP which is a hybrid of a cyclopropane σ* orbital and four π* orbitals of the cyano groups. This interaction is accompanied by the π-donation from the Cl^- p_x (-4.1 kcal mol^{-1}, 0.05 e$^-$, in plane with the cyclopropane ring) and p_y orbitals (-5.3 kcal mol^{-1}, 0.07 e$^-$, orthogonal) into linear combinations of the four cyano π* orbitals with appropriate symmetry. These interactions thus provide a clear rationale for the orbital component of the Lewis acidity of Me_2TCCP. It has to be noted that these values also contain some polarisation (mixing of filled and empty orbitals of the same fragment) which can be identified to be 1.2 kcal mol^{-1} within the A2 irreducible representation for Me_2TCCP. For [Me_2TCCP···AcO^-] the analysis is less straight forward since one of the π interactions fall into the same irreducible representation (A′) as the σ interaction, which together add up to -16.8 kcal mol^{-1} (0.08 and 0.04 e$^-$). The π interaction in plane with the cyclopropane ring (A″) amounts to -5.3 kcal mol^{-1} (0.03 e$^-$). In the case of Me_2TFCP and Me_2CP the low lying π* orbitals are absent resulting in less orbital interactions. In both cases, there is some donation into a σ* orbital of the cyclopropane ring (> 2.9 and -2.0 kcal mol^{-1}, respectively). Obviously, the capacity to accept electron density into the low lying, hybrid σ*/π* orbitals is the unique feature of Me_2TCCP responsible for the relative strong stability of its adducts in the investigated series. This is in line with a recent report about the synergistic effect that multiple cyano substituents on alkanes have on the Lewis acidity of the molecule, and that sp^3 and sp carbon centres can work in concert.[27]

While the interaction energies reported in Table 1 and Table 2 give a clear picture of the relative stabilities of the various adducts in the gas phase, such calculations ignore solvation and entropy considerations. As such, these computations are of limited value to predict actual binding in non-gaseous states such as solutions, the interior of proteins, or within cell-membranes. In an attempt to provide such guesti-

mates, the selected supramolecular reactions listed in Table 3 were considered and their Gibbs free energies were calculated using the COMSO continuous solvation model and assuming a temperature of 25 °C. The apolar hexane ($\varepsilon_r \approx 1.9$) was used as solvent, which already had an appreciable (dispersion driven) interaction energy with Me_2TCCP ($\Delta E = -5.6$ kcal mol^{-1}, see entry 2f in Table 1). An equal amount of molecules and adducts was used on both sides of the equilibria, starting from an *n*-hexane adducts and replacing *n*-hexane by a molecule bearing a lone-pair of electrons. This approach was used in order to minimize errors in the frequency calculations, particularly in the rotational and translational components of the entropy. The ΔG values of the adducts listed in Table 3 are between 3–7 kcal mol^{-1} less stabilizing than the gas-phase interaction energies (ΔE). The general trends are similar and a more negative ΔE correlates well with a more negative ΔG ($r^2 = 0.94$, see Figure S6).

In entries 1–4 of Table 3, *n*-hexane was replaced by dimethyl ether to form a hydrogen bonding adduct [MeOH···OMe_2] (entry 1), or to form tetrel-bonded adducts with Me_2TFCP, Me_2CP and Me_2TCCP (entries 2–4 respectively). The OMe_2 adducts with Me_2TFCP and Me_2CP are hardly favoured with ΔG < 1 kcal mol^{-1} and the accompanying association constants (K_a) of < 5 M^{-1} would barely be measurable.[28] The Gibbs free energies obtained for the OMe_2 adducts with methanol (~ 4 kcal mol^{-1}) and Me_2TCCP (~ 5 kcal mol^{-1}) are similar and binding in the order of $K_a = 10^3$ M^{-1} should be quantifiable with a technique such as an NMR titration.

Shown in entries 5–9 of Table 3 are the data obtained for Me_2TCCP binding to other electron rich molecules. The Gibbs free energy for SMe_2, NMe_3 and PMe_3 (entries 5–7) are similar to the data with OMe_2 with $\Delta G \approx$ 4-5 kcal mol^{-1} and K_a is in the order of 10^3 M^{-1}. The most stable adduct was found with the highly polarized $OPMe_3$ ($\Delta G = -8.6$ kcal mol^{-1}, entry 8). The second most stable is [Me_2TCCP···THF] with $\Delta G = -6.6$ kcal mol^{-1} (entry 9), which has been observed experimentally.[19]

Whether these Gibbs free energies are accurate was evaluated based on literature values found for simple bimolecular associations where the adduct is held together by a single hydrogen bonding interaction. For example, hydrogen bonding between *p*-cresol and *p*-methylpyridine has been measured at 19 M^{-1} in $CDCl_3$ ($\Delta G = -1.75$ kcal mol^{-1})[29] and one of the strongest charge neutral hydrogen bonds between perfluoro-*t*-

Table 3. Overview of calculations to estimate the Gibbs free energy (ΔG) of indicated equilibria at 298.15 K at the B3LYP-D3/def2-TZVP level of theory with a COSMO solvation model for *n*-hexane. The related association constants (K_a in M^{-1}) are also listed, as well as the gas-phase interaction energies (ΔE) of the adducts on the right-hand side of the equilibria. Energies are in kcal mol^{-1}.

Entry	Equilibrium					ΔG	K_a	ΔE
1	[MeOH···*n*-Hex]	+ OMe_2	⇆	[MeOH···OMe_2]	+ *n*-Hex	−4.14	1.09×10^3	−7.1
2	[Me_2TFCP···*n*-Hex]	+ OMe_2	⇆	[Me_2TFCP···OMe_2]	""	−0.90	4.6	−3.8
3	[Me_2CP···*n*-Hex]	+ OMe_2	⇆	[Me_2CP···OMe_2]	""	−0.39	1.9	−3.5
4	[Me_2TCCP···*n*-Hex]	+ OMe_2	⇆	[Me_2TCCP···OMe_2]	""	-5.28	7.41×10^3	-9.7
5	""	+ SMe_2	⇆	[Me_2TCCP···SMe_2]	""	-4.08	0.98×10^3	-9.3
6	""	+ NMe_3	⇆	[Me_2TCCP···NMe_3]	""	−4.45	1.84×10^3	−10.4
7	""	+ PMe_3	⇆	[Me_2TCCP···PMe_3]	""	−4.30	1.43×10^3	−8.9
8	""	+ $ONMe_3$	⇆	[Me_2TCCP···$ONMe_3$]	""	−8.63	$2.12\ 10^6$	−15.3
9	""	+ THF	⇆	[Me_2TCCP···THF]	""	−6.62	7.12×10^4	−11.2

buthanol and tri-*n*-buthylphosphaneoxide has been reported at about 2700 M^{-1} in $CDCl_3$ ($\Delta G = -4.68$ kcal mol^{-1}).[30] Calculations of both these hydrogen bonding adducts using the same methodology (but using $CDCl_3$) gave $\Delta G = -3.0$ and -6.7 kcal mol^{-1} respectively. These data imply an overestimation of the calculation method of about a factor 1.5. This would still entail an easily measurable binding of [MeOH···OMe_2] with a K_a of about 750 M^{-1}. Similarly, the various Me_2TCCP adducts would have a K_a ranging from about 10^2–10^6 M^{-1}.

Summary and concluding remarks

In summary, our calculations indicate that formation of charge neutral adducts with Me_2TCCP in solution can be thermodynamically stable and is driven largely by the balance of London dispersion forces. With increasing polarity of the interacting partner however, the orbital interactions become more important and actually dominate by far in anionic adducts. A comparison with other types of interactions show that Me_2TCCP adducts are more stable than simple hydrogen bonding with water, but less stable than traditional Lewis adducts involving Me_3B, or a strong halogen bond such as with Br_2. Several bonding analyses showed that the locus of interaction is found near the electron poor sp^3-hydridized $(NC)_2C$–$C(CN)_2$ carbon atoms. Moreover, linear combinations of the low-lying, empty CN-π^* and CC-σ^* orbitals enable Me_2TCCP to accept electron density. This donor-acceptor interaction is responsible for the remarkable relative stability of its adducts. We thus conclude that Me_2TCCP represents a rare case of a C-centred Lewis acid with acceptor hybrid σ^*/π^* orbitals. The interaction of Me_2TCCP with donor molecules is therefore on the borderline between classical dipole interactions on one hand and Lewis acid/base interactions on the other.

Experimental Section

Geometry optimizations were performed using Density Functional Theory (DFT) calculations with Spartan 2016 at the B3LYP[31]-D3[32]/def2-TZVP[33] level of theory, which is known to give accurate results at reasonable computational cost and a very low basis set superposition error (BSSE).[32–33] Molecular fragments of adducts were manually oriented in a suitable constellation before starting an unconstrained geometry optimization. Geometries and energies are listed in Table S1 ('monomers') and Table S2 (adducts). These energies were used to compute interaction energies by subtracting the energy of the individual molecules (also geometry optimized) from that of the adduct. These energies are not reported in the main text, but correlate very well with interaction energies obtained with ADF relative to geometries in the adduct (see below and Figure S2).

The geometries thus obtained were further analysed with the Amsterdam Density Functional (ADF)[34] modelling suite at the B3LYP[31]-D3[32]/TZ2P[33] level of theory (no frozen cores). This gave the reported energy decomposition and 'atoms in molecules'[35] analyses (using the default ADF settings). The accompanying interaction energies (ΔE) are reported in the main text and are relative to the geometries in the adducts, but correlate very well to the interaction energies obtained with Spartan relative to geometry optimized components (see Figure S2).

Details of the Morokuma-Ziegler inspired energy decomposition scheme used in the ADF-suite have been reported elsewhere[34,36] and the scheme has proven useful to evaluate hydrogen bonding interactions.[16b,21b] The analysis of orbital interactions was conducted with ADF and visualized with the 'view levels' option. And the NCI analyses and projections of the Laplacians were rendered using the GUI accompanying the ADF suite. The adducts in Figure 4 were optimized in ADF by imposing the appropriate symmetry in order to ease the analysis of binding mechanisms.

The Gibbs free energies (ΔG, at 298.15 K) listed in Table 3 were computed using the frequency calculation option in Spartan 2016 after geometry optimizing the molecules and adducts with COSMO solvent correction for *n*-hexane (DFT/B3LYP-D3/def2-TZVP level of theory, see Table S3 for coordinates, energies and first three vibrational frequencies). Using ADF to compute ΔG for the [Me_2TCCP···OMe_2] adduct (–5.28 kcal mol^{-1}, see entry 4 in Table 3) gave –4.05 and –4.88 kcal mol^{-1} using TZ2P and QZ4P respectively (with B3LYP-D3 and scalar relativity). As ADF ran approximately an order of magnitude slower giving about the same values (particularly with QZ4P), the values in the table were computed using Spartan 2016 (which already took more than a day to complete per entry running on 32 cores operating at 4 MHz).

Acknowledgements

The work was conducted with funds from the research program 'VIDI' with project number 723.015.006, which is financed by the Nederlandse Organisatie voor Wetenschappelijk Onderzoek (Netherlands Organization for Scientific Research, NWO).

Conflict of Interest

The authors declare no conflict of interest.

Keywords: noncovalent interactions · intermolecular interaction · tetrel bonding · density functional calculation · molecular recognition

[1] a) P. J. Cragg, *Supramolecular Chemistry: From Biological Inspiration to Biomedical Applications*, 1 ed., Springer, Dordrecht, **2010**; b) A. Bauza, T. J. Mooibroek, A. Frontera, *ChemPhysChem* **2015**, *16*, 2496–2517.

[2] a) E. Arunan, G. R. Desiraju, R. A. Klein, J. Sadlej, S. Scheiner, I. Alkorta, D. C. Clary, R. H. Crabtree, J. J. Dannenberg, P. Hobza, H. G. Kjaergaard, A. C. Legon, B. Mennucci, D. J. Nesbitt, *Pure Appl. Chem.* **2011**, *83*, 1637–1641; b) E. Arunan, G. R. Desiraju, R. A. Klein, J. Sadlej, S. Scheiner, I. Alkorta, D. C. Clary, R. H. Crabtree, J. J. Dannenberg, P. Hobza, H. G. Kjaergaard, A. C. Legon, B. Mennucci, D. J. Nesbitt, *Pure Appl. Chem.* **2011**, *83*, 1619–1636; c) G. R. Desiraju, *Acta Crystallogr. Sect. A* **2017**, *73*, C308–C308.

[3] a) H. J. Schneider, *Supramolecular Systems in Biomedical Fields*, 1 ed., RSC Publishing, Cambridge, UK, **2013**; b) T. Steiner, *Angew. Chem. Int. Ed.* **2002**, *41*, 48–76; *Angew. Chem.* **2002**, *114*, 50–80; c) P. Metrangolo, H. Neukirch, T. Pilati, G. Resnati, *Acc. Chem. Res.* **2005**, *38*, 386–395; d) S. J. Grabowski, *Hydrogen Bonding: New Insights*, Springer, Heidelberg, **2006**; e) M. R. Scholfield, C. M. Vander Zanden, M. Carter, P. S. Ho, *Protein Sci.* **2013**, *22*, 139–152; f) G. R. Desiraju, P. S. Ho, L. Kloo, A. C. Legon, R. Marquardt, P. Metrangolo, P. Politzer, G. Resnati, K. Rissanen, *Pure Appl. Chem.* **2013**, *85*, 1711–1713.

[4] a) P. Politzer, J. S. Murray, P. Lane, *Int. J. Quantum Chem.* **2007**, *107*, 3046–3052; b) A. Bauza, T. J. Mooibroek, A. Frontera, *ChemPhysChem* **2015**, *16*, 2496–2517.
[5] a) S. J. Grabowski, *Phys. Chem. Chem. Phys.* **2013**, *15*, 7249–7259; b) S. Scheiner, *Acc. Chem. Res.* **2013**, *46*, 280–288; c) P. Politzer, J. S. Murray, *ChemPhysChem* **2013**, *14*, 278–294; d) P. Politzer, J. S. Murray, T. Clark, G. Resnati, *Phys. Chem. Chem. Phys.* **2017**, *19*, 32166–32178.
[6] A. Bauza, T. J. Mooibroek, A. Frontera, *Chem. Rec.* **2016**, *16*, 473–487.
[7] R. H. Crabtree, *Chem. Soc. Rev.* **2017**, *46*, 1720–1729.
[8] A. Bauza, I. Alkorta, J. Elguero, T. J. Mooibroek, A. Frontera, *Angew. Chem. Int. Ed.* **2020**, *59*, 17482–17487; *Angew. Chem.* **2020**, *132*, 17635–17640.
[9] C. B. Aakeroy, D. L. Bryce, G. Desiraju, A. Frontera, A. C. Legon, F. Nicotra, K. Rissanen, S. Scheiner, G. Terraneo, P. Metrangolo, G. Resnati, *Pure Appl. Chem.* **2019**, *91*, 1889–1892.
[10] K. Strakova, L. Assies, A. Goujon, F. Piazzolla, H. V. Humeniuk, S. Matile, *Chem. Rev.* **2019**, *119*, 10977–11005.
[11] S. Benz, M. Macchione, Q. Verolet, J. Mareda, N. Sakai, S. Matile, *J. Am. Chem. Soc.* **2016**, *138*, 9093–9096.
[12] a) M. Macchione, A. Goujon, K. Strakova, H. V. Humeniuk, G. Licari, E. Tajkhorshid, N. Sakai, S. Matile, *Angew. Chem. Int. Ed.* **2019**, *58*, 15752–15756; *Angew. Chem.* **2019**, *131*, 15899–15903; b) A. Goujon, A. Colom, K. Strakova, V. Mercier, D. Mahecic, S. Manley, N. Sakai, A. Roux, S. Matile, *J. Am. Chem. Soc.* **2019**, *141*, 3380–3384; c) A. Colom, E. Derivery, S. Soleimanpour, C. Tomba, M. Dal Molin, N. Sakai, M. Gonzalez-Gaitan, S. Matile, A. Roux, *Nat. Chem.* **2018**, *10*, 1118–1125.
[13] S. Benz, J. L. Lopez-Andarias, J. Mareda, N. Sakai, S. Matile, *Angew. Chem. Int. Ed.* **2017**, *56*, 812–815; *Angew. Chem.* **2017**, *129*, 830–833.
[14] a) S. J. Grabowski, *Chem. Eur. J.* **2013**, *19*, 14600–14611; b) J. S. Murray, P. Lane, P. Politzer, *J. Mol. Model.* **2009**, *15*, 723–729.
[15] a) J. Langer, S. Matejcik, E. Illenberger, *Phys. Chem. Chem. Phys.* **2000**, *2*, 1001–1005; b) J. Mikosch, S. Trippel, C. Eichhorn, R. Otto, U. Lourderaj, J. X. Zhang, W. L. Hase, M. Weidemuller, R. Wester, *Science* **2008**, *319*, 183–186; c) S. Pierrefixe, J. Poater, C. Im, F. M. Bickelhaupt, *Chem. Eur. J.* **2008**, *14*, 6901–6911.
[16] a) V. R. Mundlapati, D. K. Sahoo, S. Bhaumik, S. Jena, A. Chandrakar, H. S. Biswal, *Angew. Chem. Int. Ed.* **2018**, *57*, 16496–16500; *Angew. Chem.* **2018**, *130*, 16734–16738; b) T. J. Mooibroek, *Molecules* **2019**, *24*, Art. Nr. 3370; c) J. Dutta, D. Kumar Sahoo, S. Jena, K. D. Tulsiyan, H. S. Biswal, *Phys. Chem. Chem. Phys.* **2020**, DOI: 10.1039/D1030CP00330 A.
[17] a) Q. Z. Li, H. Y. Zhuo, H. B. Li, Z. B. Liu, W. Z. Li, J. B. Cheng, *J. Phys. Chem. A* **2015**, *119*, 2217–2224; b) S. Scheiner, *J. Phys. Chem. A* **2018**, *122*, 7852–7862; c) D. Sethio, V. Oliveira, E. Kraka, *Molecules* **2018**, *23*, Art. Nr. 2763; d) Y. X. Wei, Q. Z. Li, *Mol. Phys.* **2018**, *116*, 222–230; e) K. B. Wiberg, W. F. Bailey, K. M. Lambert, *J. Org. Chem.* **2019**, *84*, 5783–5789.
[18] a) A. Bauza, A. Frontera, T. J. Mooibroek, *Phys. Chem. Chem. Phys.* **2016**, *18*, 1693–1698; b) A. Bauza, T. J. Mooibroek, A. Frontera, *Chem. Eur. J.* **2014**, *20*, 10245–10248.
[19] a) J. J. Roeleveld, S. J. L. Deprez, A. Verhoofstad, A. Frontera, J. I. van der Vlugt, T. J. Mooibroek, *Chem. Eur. J.* **2020**, *26*, 10126–10132; b) V. L. Heywood, T. P. J. Alford, J. J. Roeleveld, S. J. L. Deprez, A. Verhoofstad, J. I. van der Vlugt, S. R. Domingos, M. Schnell, A. P. Davis, T. J. Mooibroek, *Chem. Sci.* **2020**, *11*, 5289–5293.
[20] a) Y. R. Mo, J. L. Gao, S. D. Peyerimhoff, *J. Chem. Phys.* **2000**, *112*, 5530–5538; b) M. J. S. Phipps, T. Fox, C. S. Tautermann, C. K. Skylaris, *Chem. Soc. Rev.* **2015**, *44*, 3177–3211; c) P. F. Su, H. Li, *J. Chem. Phys.* **2009**, *131*, Art. Nr. 014102; d) S. Scheiner, *J. Chem. Phys.* **2020**, *153*, Art. Nr. 140901.
[21] a) J. F. Beck, Y. R. Mo, *J. Comput. Chem.* **2007**, *28*, 455–466; b) S. C. C. van der Lubbe, C. F. Guerra, *Chem. Asian J.* **2019**, *14*, 2760–2769.
[22] a) D. J. R. Duarte, G. L. Sosa, N. M. Peruchena, *J. Mol. Model.* **2013**, *19*, 2035–2041; b) J. Thirman, E. Engelage, S. M. Huber, M. Head-Gordon, *Phys. Chem. Chem. Phys.* **2018**, *20*, 905–915.
[23] a) L. Pauling, *The Nature of the Chemical Bond*, 3rd ed., Cornell University Press, Ithaca, NY, **1960**; b) C. E. Housecroft, A. G. Sharpe, *Inorganic Chemistry*, 5th ed., Pearson Education Limited, **2018**.
[24] a) J. S. Murray, P. Lane, T. Clark, K. E. Riley, P. Politzer, *J. Mol. Model.* **2012**, *18*, 541–548; b) M. Watt, L. K. E. Hardebeck, C. C. Kirkpatrick, M. Lewis, *J. Am. Chem. Soc.* **2011**, *133*, 3854–3862; c) C. D. Sherrill, *Acc. Chem. Res.* **2013**, *46*, 1020–1028; d) S. E. Wheeler, *Acc. Chem. Res.* **2013**, *46*, 1029–1038; e) S. E. Wheeler, J. W. G. Bloom, *J. Phys. Chem. A* **2014**, *118*, 6133–6147; f) L. X. Yang, J. B. Brazier, T. A. Hubbard, D. M. Rogers, S. L. Cockroft, *Angew. Chem. Int. Ed.* **2016**, *55*, 912–916; *Angew. Chem.* **2016**, *128*, 924–928; g) S. Grimme, *Angew. Chem. Int. Ed.* **2008**, *47*, 3430–3434; *Angew. Chem.* **2008**, *120*, 3478–3483; h) T. J. Mooibroek, *ChemPhysChem* **2021**, *22*, 141–153; i) K. E. Riley, J. S. Murray, J. Fanfrlik, J. Rezac, R. J. Sola, M. C. Concha, F. M. Ramos, P. Politzer, *J. Mol. Model.* **2011**, *17*, 3309–3318; j) K. E. Riley, J. S. Murray, J. Fanfrlik, J. Rezac, R. J. Sola, M. C. Concha, F. M. Ramos, P. Politzer, *J. Mol. Model.* **2013**, *19*, 4651–4659; k) S. J. Grabowski, *Chem. Rev.* **2011**, *111*, 2597–2625.
[25] a) M. V. Vener, A. N. Egorova, A. V. Churakov, V. G. Tsirelson, *J. Comput. Chem.* **2012**, *33*, 2303–2309; b) I. Mata, I. Alkorta, E. Espinosa, E. Molins, *Chem. Phys. Lett.* **2011**, *507*, 185–189; c) A. Bauza, A. Frontera, *ChemPhysChem* **2020**, *21*, 26–31; d) E. Espinosa, E. Molins, C. Lecomte, *Chem. Phys. Lett.* **1998**, *285*, 170–173.
[26] P. S. V. Kumar, V. Raghavendra, V. Subramanian, *J. Chem. Sci.* **2016**, *128*, 1527–1536.
[27] S. Scheiner, *Molecules* **2020**, *25*, Art. Nr.: 4495.
[28] Depending on the limiting values separating the measured property of unbound host versus that of a host-guest complex (e.g. chemical shifts in NMR).
[29] C. C. Robertson, J. S. Wright, E. J. Carrington, R. N. Perutz, C. A. Hunter, L. Brammer, *Chem. Sci.* **2017**, *8*, 5392–5398.
[30] a) J. L. Cook, C. A. Hunter, C. M. R. Low, A. Perez-Velasco, J. G. Vinter, *Angew. Chem. Int. Ed.* **2007**, *46*, 3706–3709; *Angew. Chem.* **2007**, *119*, 3780–3783; b) Literature data in hexane solution for hydrogen bonding of bimolecular association involving a single hydrogen bond could not be found.
[31] a) A. D. Becke, *Phys. Rev. A* **1988**, *38*, 3098–3100; b) C. T. Lee, W. T. Yang, R. G. Parr, *Phys. Rev. B* **1988**, *37*, 785–789.
[32] S. Grimme, J. Antony, S. Ehrlich, H. Krieg, *J. Chem. Phys.* **2010**, *132*, Art. Nr. 154104.
[33] a) F. Weigend, R. Ahlrichs, *Phys. Chem. Chem. Phys.* **2005**, *7*, 3297–3305; b) F. Weigend, *Phys. Chem. Chem. Phys.* **2006**, *8*, 1057–1065.
[34] G. te Velde, F. M. Bickelhaupt, E. J. Baerends, C. F. Guerra, S. J. A. van Gisbergen, J. G. Snijders, T. Ziegler, *J. Comput. Chem.* **2001**, *22*, 931–967.
[35] R. F. W. Bader, *Acc. Chem. Res.* **1985**, *18*, 9–15.
[36] F. M. Bickelhaupt, E. J. Baerends, in *Reviews in Computational Chemistry, Vol 15, Vol. 15* (Eds.: K. B. Lipkowitz, D. B. Boyd), Wiley-Vch, Inc, New York, **2000**, pp. 1–86.

Manuscript received: June 4, 2021
Revised manuscript received: July 18, 2021
Accepted manuscript online: July 27, 2021
Version of record online: August 19, 2021